Nanoscale

Accepted Manuscript

This article can be cited before page numbers have been issued, to do this please use: Y. Oh and Q. Cui, *Nanoscale*, 2023, DOI: 10.1039/D3NR00930K.

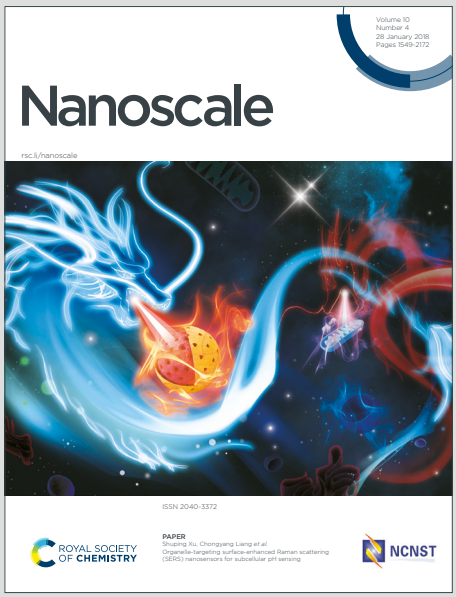

ROYAL SOCIETY OF CHEMISTRY

rsc.li/nanoscale

View Article Online
DOI: 10.1039/D3NR00930K

Non-equilibrium transport of nanoparticles across the lipid membrane

Younghoon Oh† and Qiang Cui*,†,‡

†*Department of Chemistry, Boston University, 590 Commonwealth Avenue Boston, MA 02215*

‡*Departments of Physics and Biomedical Engineering, Boston University, 590 Commonwealth Avenue Boston, MA 02215*

E-mail: qiangcui@bu.edu, Tel:(+1)-617-353-6189

Abstract

Development of effective strategies for the internalization of nanoparticles is essential in many applications, such as drug delivery. Most, if not all, previous studies are based on equilibrium considerations. In this work, inspired by the recent development of a pro-drug delivery strategy based on reversible esterification, we consider a non-equilibrium transport mechanism for nanoparticles of a 6 nm diameter across the lipid membrane. We divide the transport process into insertion and ejection steps, which are studied with coarse-grained models using free energy and reactive Monte Carlo simulations, respectively. The simulations show that the non-equilibrium transport efficiency is relatively insensitive to the fraction of reactive surface ligands once a modest threshold is surpassed, while the distribution pattern of different (hydrophilic, reactive and permanent hydrophobic) ligands on the nanoparticle surface has a notable impact on both the insertion and ejection steps. Our study thus supports a novel avenue for designing nanoparticles that are able to be efficiently internalized and provides a set of relevant guidelines for surface functionalization.

View Article Online
DOI: 10.1039/D3NR00930K

1 Introduction

Due to rapid progress in synthesis and surface functionalization, nanoparticles have emerged as promising materials in various bioimaging and biomedicine applications, such as drug delivery.[1,2] In many such applications, an important challenge is to design strategies that facilitate the transport of nanoparticles across the cell membrane, which constitutes a major barrier for the internalization of molecular and macromolecular species.[3,4] Accordingly, considerable research efforts have been focused on understanding how various properties of nanoparticles impact the transport process, including the effects of size,[5–9] shape,[7,9–14] surface ligand charge and flexibility[15–19], mechanical stiffness[20,21] and co-operativity[22–25] of nanoparticles. Modification of nanoparticle surface that might favor membrane wrapping and therefore transport across the membrane has also been extensively analyzed.[26–29]

Most, if not all, of the previous analyses, however, were conducted in an equilibrium framework, by considering, for example, the competition between membrane bending free energy and membrane-nanoparticle adhesion.[30–32] In nature, many cellular internalization processes are non-equilibrium in character. Chaperon-assisted translocation of peptide chains is a representative example.[33–35] When a peptide chain initiates the translocation through a pore in the cell membrane, chaperone proteins are attached to the protein, preventing the peptide from detaching from the pore. The attached chaperone acts as a thermal ratchet to bias the translocation of the peptide across the pore while overcoming the free energy barrier that mainly originates from conformational entropy.[27,36–43]

Motivated in part by the thermal ratchet mechanism, the Raines group has developed an ingenious chemical biological approach for transporting proteins (pro-drugs) across cell membranes.[44–47] The approach esterifies anionic groups (aspartates and glutamates) on the protein surface, which helps to reduce the anionic charges that hamper the protein from approaching and being partitioned into the cell membrane; functional groups used in the esterification can be selected (e.g., in terms of hydrophobicity) to fine-tune the partitioning of the protein into the cell membrane. Once the modified protein is in the membrane, some

View Article Online
DOI: 10.1039/D3NR00930K

of the esterified groups are accessible to the cytosol, which contains enzymes that convert them back to the anionic carboxylates, leading to a barrier for the protein to diffuse back to the exterior of the cell. In other words, progressive de-esterification forms a "thermal ratchet" that helps to bias the protein to translocate into the cytosol, following a mechanism reminiscent of that for the chaperon-assisted peptide translocation across the membrane.

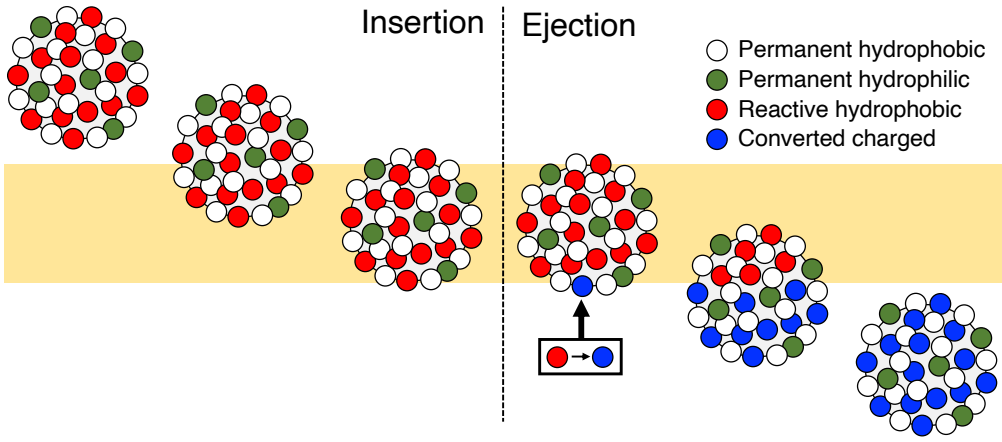

Figure 1: A schematic illustration for the non-equilibrium transport of nanoparticle across the lipid membrane. When reactive hydrophobic ligands (red) become exposed to the "cytosolic" side of the membrane (shaded dark yellow), they are converted into hydrophilic ligands by enzymes, leading to an energetic barrier for the nanoparticle to diffuse back to the "extracellular" side of the membrane. As more reactive ligands undergo the conversion, the nanoparticle preferentially translocates into the cytosol.

Inspired by the work of Raines and co-workers on protein transport,[44–47] we explore a similar strategy for facilitating nanoparticle transport across the membrane (Fig. 1). By installing esterified carboxylate (or other reversibly reactive) surface ligands, we anticipate that the thermal-ratchet mechanism will serve as a novel pathway for nanoparticle internalization. The minimal set of design parameters in this context includes the fraction of esterified carboxylate surface ligands and their spatial distributions. Indeed, it might be challenging to install a large number of esterified carboxylate ligands on the nanoparticle surface,[47] thus establishing the sensitivity of the transport efficiency to the fraction and distribution of such reactive ligands will provide valuable guidance to the design. Moreover, the mechanistic insights we glean will also be instructive to the further development of the

View Article Online
DOI: 10.1039/D3NR00930K

approach for protein internalization.

In this work, we explore the problem using coarse-grained models so as to focus on the most salient physical features and principles. In particular, we divide the process into two steps: insertion (partitioning) of the nanoparticle into the lipid membrane, and transport ("ejection") of the nanoparticle to the inner side of the membrane (see below) via the ratcheting mechanism. The insertion step is modeled with the popular coarse-grained MARTINI model,[48] while the ratcheting ejection step is analyzed using reactive Monte Carlo and a further simplified representation of the membrane. We find that the non-equilibrium transport efficiency is relatively insensitive to the fraction of reactive surface ligands once a modest threshold is surpassed, while the distribution pattern of ligands has a notable impact on both the insertion and ejection steps, highlighting the importance of rational design of surface functionalization.

2 Computational Models and Methods

We employ coarse-grained models (Fig. 2) to investigate the non-equilibrium transport mechanism of the nanoparticle across the membrane. For simplicity, the surface functionalization pattern is represented by the different parameter types of the surface beads. In general, we distinguish two types of surface beads: hydrophobic and hydrophilic, which favor membrane interior and bulk solution, respectively. We assume that the esterified ligands are hydrophobic in nature, and converted to be hydrophilic following the reaction (see below). We vary the fraction and distribution of reactive hydrophobic groups to mimic different esterification patterns of surface ligands (Fig. 2c, d).

The transport process is separated into two steps: insertion of the nanoparticle from the "extracellular" side into the membrane, and ejection of the nanoparticle via the thermal ratchet process into the cytosolic side. During the insertion step (Fig. 2a), no reaction is considered and thus we only distinguish two types of surface beads, hydrophobic (colored

View Article Online
DOI: 10.1039/D3NR00930K

white) and hydrophilic (colored green), and we characterize the insertion process by free energy simulations using the MARTINI model, which describes both lipid molecules and water explicitly. For the ejection step (Fig. 2b), we employ reactive Monte Carlo simulations[49] and a further simplified (implicit) treatment of the membrane and water (see below). During these simulations, some of the hydrophobic beads (colored red) are converted to hydrophilic ones (colored blue) once they become accessible to the cytosolic side, which is meant to mimic the de-esterfication process catalyzed by enzymes present in the cytosol.[47]

2.1 Insertion: MARTINI simulations

The MARTINI 2.2 force field model[50] is used to describe the insertion process of nanoparticles with different surface functionalization patterns. The nanoparticle has a diameter of 6 nm, similar in size to proteins[46,47] and various nanoparticles[19,21] studied in recent work, and is constructed with harmonic constraints between neighboring beads (using a force constant 2000 $kJ\ mol^{-1}\ nm^{-2}$) to maintain the structural integrity. To further ensure the rigidity of the nanoparticle, we also introduce virtual beads at the center of the hollow nanoparticle. The distance between the virtual bead and each surface bead is harmonically constrained with a force constant of 3000 $kJ\ mol^{-1}\ nm^{-2}$. Since no reaction is considered in the insertion step, only hydrophobic (white) and hydrophilic (green) surface beads are considered, which are described with the C1 and Qd MARTINI beads, respectively. The fraction of hydrophilic beads is fixed to be 36.4% for all particle types, leading to 202 hydrophobic and 117 hydrophilic beads, respectively; the fraction 36.4% is chosen based on the remaining number of negatively charged surface residues after esterification in the protein studied by Raines and co-workers.[47] For the random and Janus nanoparticles, the hydrophilic beads are distributed randomly around the entire nanoparticle (random) and around a hemisphere (Janus), respectively. Hydrophilic beads are partially charged with -0.1e (114 beads) or -0.2e (3 beads) to make the total charge of the nanoparticle an integer; the small magnitudes of the partial charges were chosen to attenuate the limited accuracy of coarse-grained models

View Article Online
DOI: 10.1039/D3NR00930K

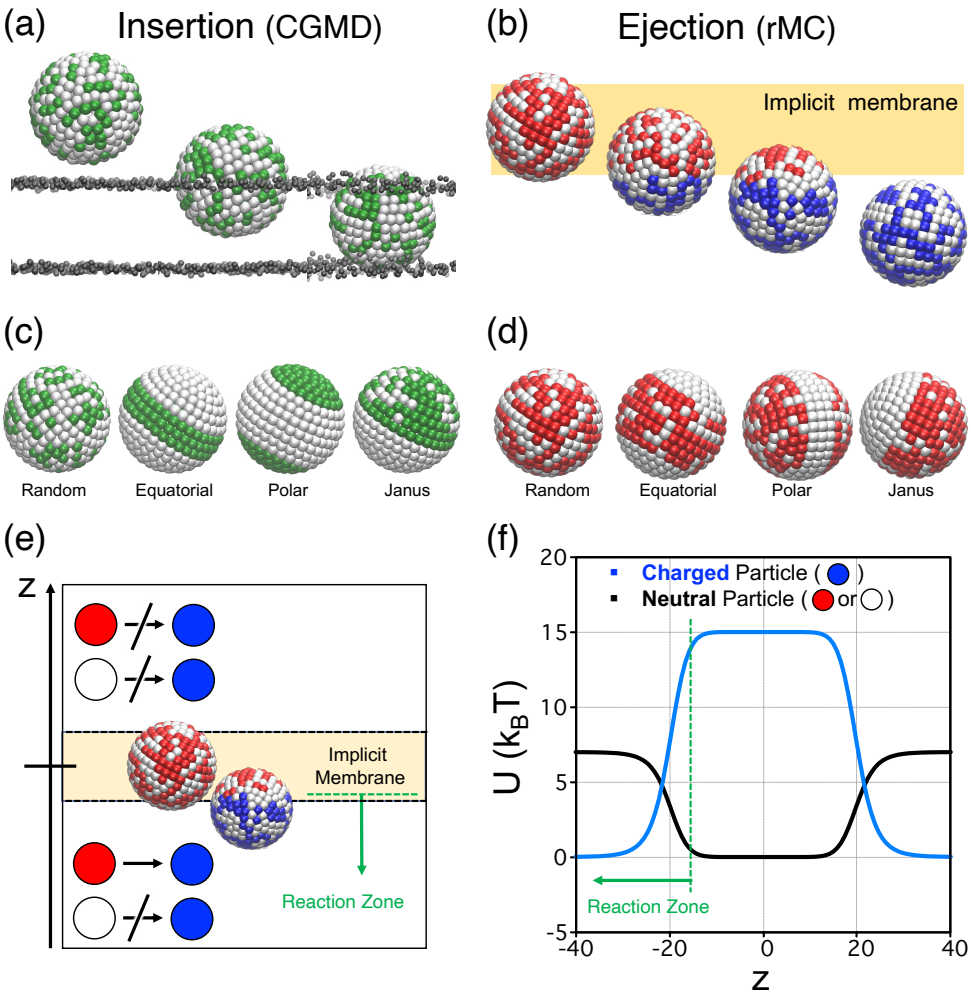

Figure 2: Illustration for the computational models and methods explored in this work for the analysis of nanoparticle translocation. Coarse-grained simulation snapshots of (a) the insertion (lipids and water not shown for clarity) and (b) reactive "ejection" steps of the translocation process. The insertion step is studied with the MARTINI model, and the ejection step is studied with reactive Monte Carlo (rMC) and a further simplified treatment of membrane. Different distribution patterns of surface ligands are studied for both the (c) insertion and (d) ejection steps. For insertion, random, equatorial, polar, and janus distributions of hydrophilic (green) and hydrophobic (white) ligands are studied; for ejection, the four distributions are for the reactive (red) and non-reactive (white) hydrophobic ligands. (e-f) Key components of rMC simulations: once accessible to the cytosolic side of the implicit membrane slab, the reactive (red) hydrophobic ligands are allowed to convert into hydrophilic ones (blue); the ligands (beads) experience z-dependent potentials, which describe their energetic preferences to water or the membrane interior. While most simulations are done with the parameters shown in panel (f), other values are also explored (see discussion in text).

View Article Online
DOI: 10.1039/D3NR00930K

in treating highly charged nanoparticles[51]. Four different distributions (random, equatorial, polar, and Janus) of hydrophilic beads are studied (Fig. 2c).

The lipid bilayer contains anionic (DPPS) and zwitterionic (POPS) lipids with a molar ratio of 2:8. Lipid membranes are generated by using the MARTINI maker module of CHARMM-GUI.[52–54] The system is neutralized by adding ions (Na^+ and Cl^-) along with MARTINI water beads; additional salt ions are added to reach a physiological concentration of 0.15 M. The simulation boxes typically have the dimension of $17nm \times 17nm \times 15nm$, and contain ~ 970 lipid molecules, $\sim 28,000$ water beads, and ~ 600 neutralizing ions.

The system is simulated using the Gromacs 2018.3 package.[55] Molecular dynamics trajectories are propagated using the leap-frog algorithm[56] and a time step of 0.02 ps. During equilibration, v-rescale thermostat[57] and the Berendsen barostat[58] is used to maintain temperature and pressure, respectively. For the production simulations, the Parrinello-Rahman barostat[59] is applied. We calculate the potential mean force (PMF) for nanoparticle insertion using the distance between the nanoparticle and the membrane center of mass as the reaction coordinate. Umbrella sampling simulations are carried out with 60 (58 for the random distribution) consecutive biasing windows with an interval of $1\mathring{A}$ and a force constant of 1000 $kJ\ mol^{-1}\ nm^{-2}$. Each window is simulated for 100 ns and the PMF is constructed using WHAM;[60] three independent PMF simulations are carried out to estimate statistical errors.

2.2 Ejection: reactive Monte Carlo simulations

For the analysis of the ejection process, we perform reactive Monte Carlo (rMC) simulations[49] using the *Faunus* Monte Carlo simulation package.[61,62] In those rMC simulations, the nanoparticle is also modeled with a diameter of 6 nm and contains 319 beads. Similar to the MARTINI simulations, four different distributions of the surface ligands (random, equatorial, polar, and Janus) are analyzed; in the rMC simulations, however, the distributions concern the reactive hydrophobic residues (Fig. 2d). For each type of distribution, we also

View Article Online
DOI: 10.1039/D3NR00930K

vary the number of reactive beads, which is characterized by the fraction of surface beads being reactive (f_{react}); the value of f_{react} explored is typically between 0.01 to 0.6.

The cellular membrane and solvent are modeled implicitly by defining position-dependent (along z, the membrane normal direction) potential energies for the beads; the thickness of the implicit membrane is taken to be ∼4 nm, which is the typical thickness of the hydrophobic segment of a lipid bilayer. As shown in Fig. 2f, the potential favors the hydrophobic beads to be in the membrane interior, while it penalizes the hydrophilic beads in the membrane interior relative to the bulk solution. The order of magnitude of the energetic biases is approximately based on the insertion PMFs computed for amino acid sidechains into a zwitterionic lipid bilayer,[63] although we also explore the impact of varying the energetic bias of hydrophobic beads ($2k_BT$ or $7k_BT$).

At the beginning of the rMC simulations, the nanoparticle has two types of surface beads: permanent (white) hydrophobic beads and reactive (red) hydrophobic beads. During the rMC simulations, in addition to translation and rotation moves of the nanoparticle, the red hydrophobic beads are stochastically converted to hydrophilic ones (blue) when they are located in the "cytosolic" region (i.e., $z < -20\mathring{A}$, see Fig. 2e). Such reaction is sampled during the rMC with a large equilibrium constant of $lnK = 100$, thus making the reaction effectively irreversible.

For each nanoparticle system, 10^3 independent rMC simulations are performed for each f_{react} value to evaluate the translocation efficiency. Each rMC run contains ∼10^5 MC steps, and for each MC step, the possible moves include nanoparticle translation (with a step size of 2 Å), rotation (with a step size of 0.1 radian), and reaction.

Finally, we also probe the effect of mixing a fraction of permanent hydrophilic ligands, which are expected to reduce the stabilization of the nanoparticle in the membrane interior and therefore might facilitate the ejection step. The energetic preference of the hydrophilic bead to the bulk solvent is varied over a range of 1 to 15 k_BT.

View Article Online
DOI: 10.1039/D3NR00930K

3 Results and Discussion

3.1 Insertion free energy depends on surface polar ligand distribution

The insertion potentials of mean force (PMFs) for the nanoparticles with four surface polar ligand distributions are shown in Fig. 3, which show significantly different qualitative and quantitative trends.

With a random distribution of hydrophilic surface ligands, the insertion PMF is uphill with a significant penalty (>200 kJ/mol) for the partition of the nanoparticle into the membrane. This is expected due to the burial of a large number of hydrophilic beads in the membrane interior. Throughout the simulations, no significant deformation of the membrane or reorientation of the nanoparticle is observed (Fig. 3d).

When the hydrophilic beads are distributed in the two polar regions, the insertion PMF is largely downhill with modest barriers and a very shallow intermediate that corresponds to a partially inserted nanoparticle. In the fully inserted state (snapshot iv in Fig. 3b), the nanoparticle is oriented in the membrane similar to a typical transmembrane protein, with the hydrophobic region buried in the lipid tail region while the polar hydrophilic beads being solvent exposed. During the insertion process (snapshots i and iii in Fig. 3b), significant membrane deformation is induced whenever there is a major change in the amount of hydrophobic surface in contact with the membrane.

With the hydrophilic beads limited to the equatorial belt (Fig. 2c), the insertion PMF features a modest insertion barrier and a relatively shallow intermediate, which is followed by another barrier (∼100 kJ/mol) before reaching another local free energy minimum that corresponds to a fully inserted nanoparticle. The fully inserted state is slightly more favorable in free energy than when the nanoparticle is in the bulk solution, likely due to the fact that there is a larger number of hydrophobic surface beads that help stabilize the nanoparticle in the membrane interior.

View Article Online
DOI: 10.1039/D3NR00930K

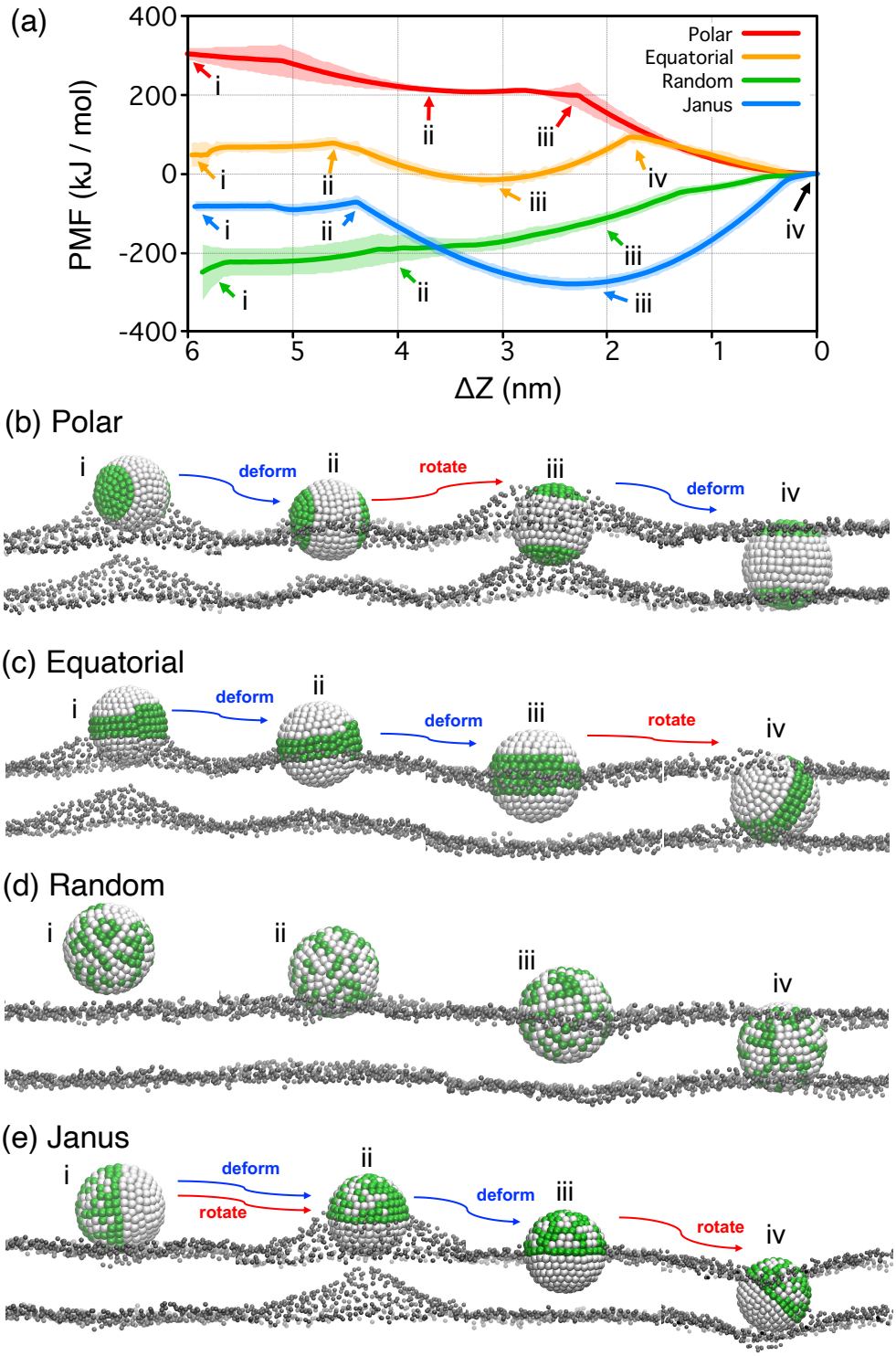

Figure 3: Insertion free energy profiles and snapshots for nanoparticles with different hydrophobic (white)/hydrophilic (green) surface ligand distributions (Fig. 2c). (a) Computed insertion potentials of mean force (PMFs) with statistical errors shown as shaded regions; the PMFs for different systems are shifted so that the fully inserted state is considered as the common reference value. Selected snapshots from different stages of insertion are shown in (b)-(e) for the different surface ligand distributions; considerable local membrane deformations are noted in many cases.

View Article Online
DOI: 10.1039/D3NR00930K

Finally, when the hydrophilic beads are distributed on one face of the Janus particle, there is a deep free energy minimum that corresponds to the state where the hydrophobic face of the particle is fully immersed in the membrane while the hydrophilic part remains largely solvent exposed (snapshot iii in Fig. 3e). Therefore, there is a significant penalty for the nanoparticle to be fully inserted, due to the burial of a significant number of hydrophilic beads in the lipid tail region.

The trends in the computed insertion PMFs suggest that the nanoparticles with hydrophilic ligands being limited to the polar or equatorial regions can readily reach the fully inserted state without any inhibiting energetic penalty. Once in the fully inserted state, the hydrophobic ligands become accessible to the "cytosolic" side of the membrane and therefore potentially be able to initiate the thermal-ratchet driven transport. With randomly distributed hydrophilic ligands or the Janus particle, however, there is a significant energetic penalty to reach the fully inserted state; as a result, when the particle size is modest, the hydrophobic ligand may not be accessible to the "cytosolic" side. Therefore, to enable the non-equilibrium transport with these two types of polar surface ligand distributions, it is essential that either the particle size is large (compared to the thickness of the bilayer) or the reactive hydrophobic ligands are sufficiently long so that they are accessible to the cytosolic side even when the particle is only partially inserted into the lipid membrane.

3.2 Non-equilibrium transport depends on reactive ligand coverage and distribution

To illustrate the non-equilibrium transport process, we first present two different scenarios of rMC simulations on a nanoparticle: successful and unsuccessful ejections. Here the nanoparticle model contains 319 surface beads and contains 50 reactive monomers with a random distribution. The diameter of nanoparticle is 6 nm, slightly larger than the thickness of the implicit membrane (4 nm). No hydrophilic surface beads are included here because their presence will make it easier for the particle to be ejected out of the membrane (*vide infra*).

View Article Online
DOI: 10.1039/D3NR00930K

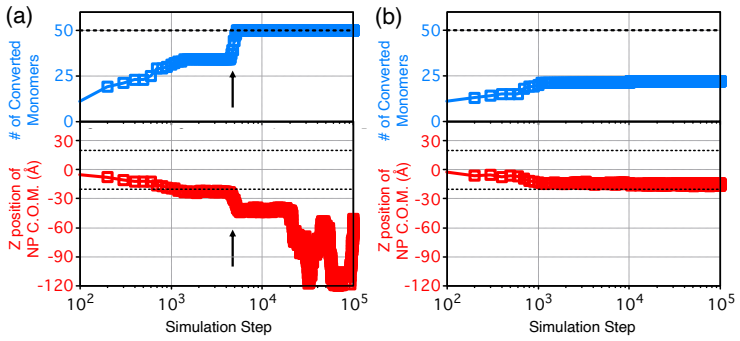

Figure 4: Illustration of different translocation trajectories from rMC simulations. Two distinct scenarios, which describe (a) successful and (b) unsuccessful ejections during rMC simulations. In both scenarios, we track the number of reacted monomers (blue) and the z coordinate of the nanoparticle center of mass (red) throughout the simulations. The dashed lines indicate the locations of the implicit membrane boundary, which has a thickness of 4 nm. The successful ejection from the implicit membrane is defined if the shortest distance from the membrane boundary and any of the monomer bead of the nanoparticle is greater than 2 Å.

As the rMC simulations proceed, we track the number of surface beads that get converted into hydrophilic ones and the z position of the nanoparticle's center of mass (Fig. 4). The two different scenarios exhibit rather different behaviors. For an unsuccessful ejection (Fig. 4b), both the number of reacted hydrophobic beads and the z location of the nanoparticle reach a plateau rather quickly, after $\sim 10^3$ MC steps, and they remain largely constant for $\sim 10^5$ MC steps. In other words, the particle remain trapped inside the membrane. By contrast, for the successful ejection (Fig. 4a), the number of reacted surface beads undergoes a rapid increase around $\sim 5 \times 10^3$ MC steps; accordingly, the z location of the nanoparticle decreases in value rapidly, representing the ejection of the particle into the cytosolic side of the membrane.

The distinct behaviors of the two different fates of the nanoparticle highlight that the fraction of reactive surface ligands plays an important role in determining the probability of successful non-equilibrium transport. Without a sufficient number of converted hydrophilic surface ligands, the nanoparticle is trapped inside the membrane by the favorable burial of hydrophobic surface groups. As discussed below, this can be alleviated by including a fraction of permanently polar surface ligands.

Following this initial illustration, we analyze more systematically the effects of the frac-

View Article Online
DOI: 10.1039/D3NR00930K

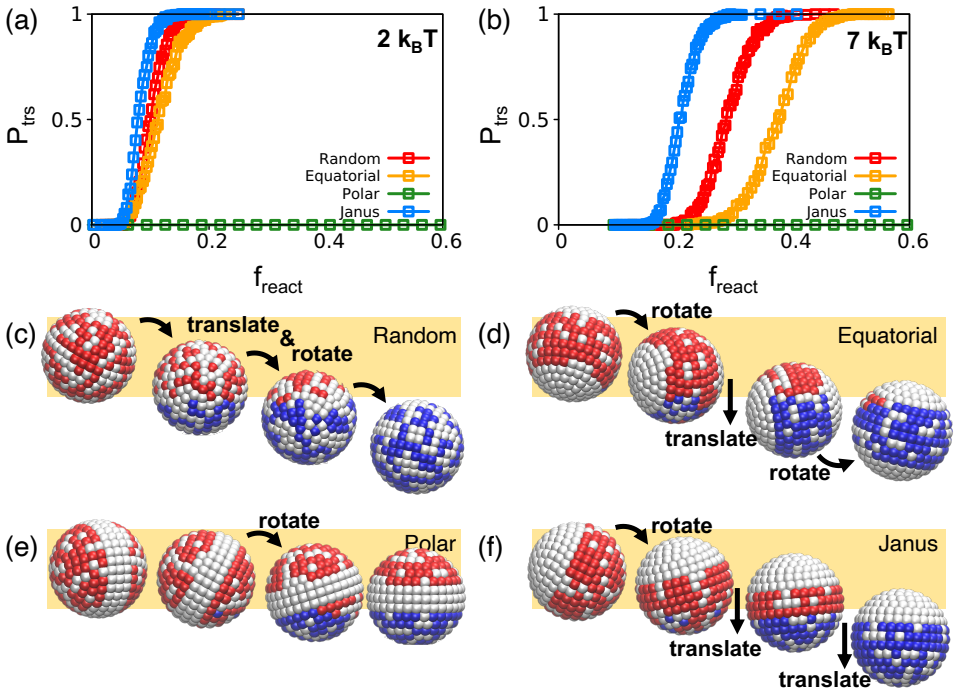

Figure 5: The probability of successful translocation P_{trs} as a function of the fraction of reactive surface hydrophobic beads, f_{react} when the free energy stabilization for a hydrophobic monomer inside the membrane is (a) $2k_BT$ and (b) $7k_BT$. The value of P_{trs} for each type of particle and f_{reac} is determined based on 10^3 independent rMC simulations, each of which includes $\sim 10^5$ MC steps. The typical ejection mechanisms are shown in (c)-(f) for the four different reactive ligand distributions.

View Article Online
DOI: 10.1039/D3NR00930K

tion and distribution of surface reactive ligands and the free energy stabilization of the hydrophobic monomers. We compare four distributions: random, equatorial, polar, and Janus (Fig. 2d); note again we focus in this section on the distribution of reactive and permanent (non-reactive) hydrophobic ligands on the nanoparticle surface, and no hydrophilic ligands are included at the start of the rMC simulations. For each ligand distribution, we also vary the fraction of reactive ligands f_{react} from 0.01 to 0.6. To compare the translocation efficiency, we perform 10^3 independent rMC simulations for each particle type; the probability of successful translocation P_{trs} is calculated by counting the fraction of rMC simulations that leads to ejection of the nanoparticle to the cytosolic side (Fig. 5). The precise value of f_{react} is affected by parameters in the simulation setup such as the thickness of the implicit membrane, threshold z position for defining the successful ejection, and transfer free energies of different bead types (Fig. 2e-f, see discussion below). Nevertheless, comparing the trends in P_{trs} for the different nanoparticles helps identify the features of surface ligands that most significantly impact the translocation efficiency.

Most nanoparticles exhibit the sigmoidal trend for P_{trs} as a function of f_{react} (Fig. 5). This is qualitatively expected, as a larger fraction of reactive surface ligands leads to a larger driving force for the nanoparticle to be ejected from the membrane interior towards the cytosolic side. The precise threshold, however, is dependent on he spatial distribution of the reactive surface ligands regardless of the transfer free energy of the hydrophobic beads. With a random distribution, for example, $f_{react} \simeq 0.35$ and $f_{react} \simeq 0.08$ when the transfer free energy is $7k_BT$ and $2k_BT$ for P_{trs} to reach 50%, respectively.

Nanoparticles with reactive surface ligands limited to the polar regions fail to get ejected for all f_{react} values explored here ($f_{react} \leq 0.5$). This is not unexpected since even after all the reactive surface ligands in the bottom of the particle get converted into the hydrophilic type, there are significantly larger number of hydrophobic surface ligands that stabilize the particle in the membrane interior. For the reactive surface ligands on the top of the particle to access the cytosolic side, the nanoparticle needs to overcome a high free energy barrier of

View Article Online
DOI: 10.1039/D3NR00930K

rotation, which is necessarily unfavorable due to bringing (reacted) hydrophilic ligands into the membrane interior. As a result, the ratchet mechanism works poorly for nanoparticles with polar distribution of reactive ligands (Fig. 5e).

The similar accessibility issue of reactive surface ligands also applies to the case when these ligands are limited to the equatorial region of the particle, although to a lesser extend than the case of polar distribution. As depicted in Fig. 5d, the nanoparticle with an equatorial distribution of reactive ligands undergoes two significant rotations. Initially, at the early stage of ejection, the nanoparticle rotates in a direction that enhances the exposure of the reactive and reacted monomers. Subsequently, upon completing the ejection process, it undergoes another rotation, during which the hydrophobic monomers in one of the polar regions become stabilized, which makes the ejection of equatorial distribution less efficient than random distribution. Nevertheless, the probability of a successful ejection is higher compared to the polar distribution, given the same number of reactive monomers. As seen from Fig. 5ab, to reach a P_{trs} value of 50%, a slightly higher value of $f_{react} \simeq 0.11$ or $f_{react} \simeq 0.38$ is required, when the free energy stabilization is $2k_BT$ and $7k_BT$, respectively.

By contrast, the Janus distribution is efficient for ejection with a single global rotation for a large number of surface ligands to react and get converted to hydrophilic ones (Fig. 5f). Since the reactive monomers are concentrated on one half of the surface region, it is more efficient compared to the random case. Even the hydrophobic monomers on the other half get stabilized inside the membrane, the nanoparticle readily gets ejected out of the membrane. To reach a P_{trs} value of 50% with the Janus reactive ligand distribution, a f_{react} value as low as 0.08 and 0.17 is required, for $2k_BT$ and $7k_BT$ free energy stabilization, respectively. Evidently, the ratchet mechanism is particularly efficient for such a ligand distribution.

As mentioned in the beginning of this section, for the rMC simulations of the ejection step, we focus mainly on nanoparticles that have a combination of reactive and permanent hydrophobic surface ligands. We also examine four models of nanoparticles that incorporate permanent hydrophilic surface beads (see Fig. 6). We consider two distributions of reactive

View Article Online
DOI: 10.1039/D3NR00930K

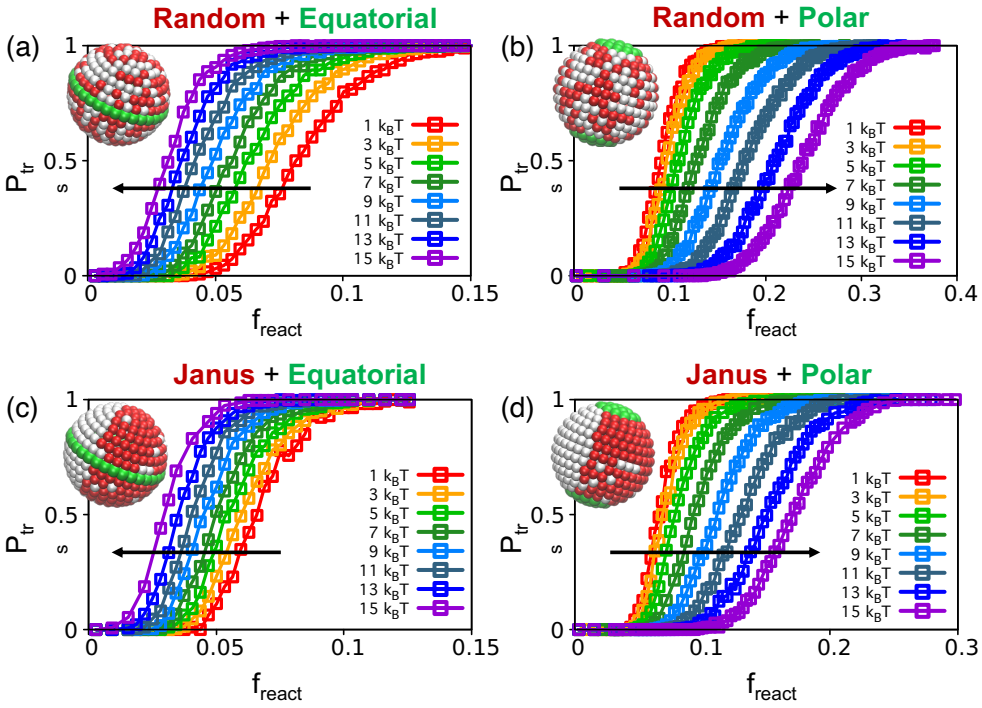

Figure 6: rMC simulations to probe the impact of the permanent hydrophilic monomers with an equatorial distribution (a,c) or a polar distribution (b,d). Reactive monomers are distributed either randomly (a,b) or with a Janus pattern (c,d). The transfer free energy of the permanent hydrophilic monomers (green) ranges from $1k_BT$ to $15k_BT$.

View Article Online
DOI: 10.1039/D3NR00930K

particles (random and Janus) that are efficient for the ejection stage, as well as two distributions of permanent hydrophilic monomers (polar and equatorial) that are advantageous for the insertion stage.

As expected, the impact of reactive monomer distribution remains consistent in the presence of permanent hydrophilic monomers. Irrespective of the arrangement of permanent hydrophilic monomers, nanoparticles with Janus reactive monomers exhibit greater ejection efficiencies compared to the random distribution of reactive ligands. However, the impact of permanent hydrophilic monomers significantly depends on their distribution. In the equatorial case, nanoparticles are ejected more effectively from the membrane as the free energy penalty of burying the hydrophilic monomers in the membrane increases. Nanoparticles with equatorial hydrophilic monomers cannot be stabilized within the membrane; therefore, a higher free energy penalty facilitates their ejection. Conversely, a polar distribution of permanent hydrophilic monomers enables nanoparticle stabilization within the membrane, leading to inefficient ejections.

3.3 Discussion: design guidelines for non-equilibrium transport

To design the surface pattern of nanoparticles for the non-equilibrium transport process, several considerations come to mind. First, the particle needs to insert into the membrane sufficiently deeply such that a considerable number of reactive ligands are accessible to the cytosolic side of the membrane to initiate enzyme catalyzed transformation of these ligands to the charged state. In this regard, the insertion PMF results (Fig. 3) suggest that even with a modest ($\sim$40%) fraction of hydrophilic beads, nanoparticles with random or Janus distribution of hydrophobic and hydrophilic surface ligands likely experience considerable energetic penalty for deep insertion. Therefore, if these functionalization patterns are pursued, either the particle size needs to be sufficiently large (compared to the membrane thickness) or the reactive surface ligands need to be sufficiently long so that they are accessible to the cytosolic side even with partial insertion of the nanoparticle into the membrane. For the

View Article Online
DOI: 10.1039/D3NR00930K

polar and equatorial distributions, the insertion process is energetically favorable, although the ejection step also needs to be carefully tuned (see below).

With the rMC simulations (Fig. 5), we are able to explore how the transport (ejection) efficiency depends on the distribution of reactive and permanent hydrophobic ligands, once the particle is inserted into the membrane. The results clearly show that the polar reactive ligand distribution with a permanent hydrophobic equatorial belt is to be avoided, while both the Janus and random distributions are better than the equatorial distribution of reactive ligands. As expected, the required fraction of surface reactive ligands depends on the energetic stabilization of hydrophobic residues by the membrane interior; a stronger stabilization requires a higher fraction of surface reactive ligands (Fig. 6a). The energetic bias can be experimentally tuned by altering the degree of hydrophobicity of surface ligands, or by mixing in hydrophilic ligands, which effectively modulate the stabilization of the particle by the membrane interior. Indeed, we see that the ejection process is influenced by the distribution of permanent hydrophilic monomers in different ways. A polar distribution tends to make the ejection inefficient, whereas an equatorial distribution facilitates the ejection.

Therefore, by combining insights from the analysis of both insertion and ejection steps, we suggest that to balance these steps, the following design rules are worthwile considering. (1). Random and Janus distributions of hydrophilic and hydrophobic surface ligands should be avoided unless the particle is large in size and/or the reactive ligands feature extended conformations; (2). Polar distribution of reactive surface ligands with a hydrophobic equatorial region should be avoided. (3) Effective functionalization patterns could be to mix hydrophilic and hydrophobic ligands with the former in the polar (Fig. 7a) or equatorial (Fig. 7b) regions, while reactive ligands are distributed in a Janus-like pattern in the hydrophobic region. With these functionalization patterns, the particles are expected to be partitioned into the membrane without major energetic penalties, and in the inserted state (shown schematically in Fig. 7), the reactive ligands are readily accessible to the cytosolic region of membrane to initiate the ejection process.

View Article Online
DOI: 10.1039/D3NR00930K

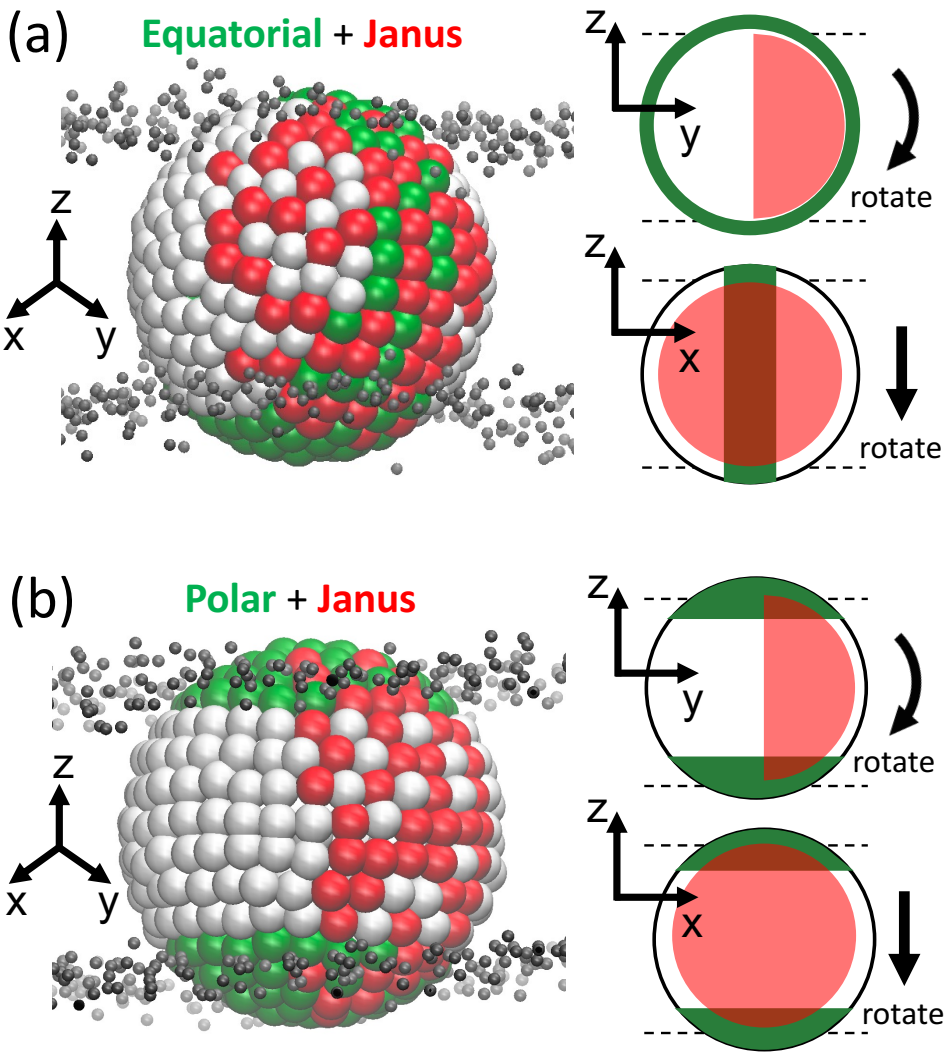

Figure 7: Examples for recommended surface ligand distributions that balance both insertion and ejection steps during the non-equilibrium driven transport. Green indicates permanent hydrophilic ligands, while red and white indicate reactive and permanent hydrophobic ligands, respectively. The snapshots illustrate the expected inserted configuration of the nanoparticles, and the schematics on the right indicate the motion of the nanoparticles as the reactive groups undergo chemical transformations that drive the translocation.

View Article Online
DOI: 10.1039/D3NR00930K

3.4 Discussion: limitations of the current models

The primary focus of our study is to establish the key physical principles that govern the efficiency of the non-equilibrium transport mechanism. Therefore, we chose to employ highly simplified models for the functionalized nanoparticles, which do not capture molecular features of the surface ligands such as volume and flexibility, which have been shown in previous studies to contribute to the interaction with lipid membrane.[15–19] However, incorporating the chemical nature of ligands explicitly in the rMC simulations poses significant computational challenges, as it would necessitate additional parameterization and including various complex Monte Carlo moves, rendering it impractical for long simulations; for the similar consideration, an implicit membrane model was used in the rMC simulations. By focusing on a minimalist coarse-grained representation of the nanoparticles, we are able to probe the effects of surface ligand (both reactive and non-reactive) distributions on the transport efficiency, without convoluting contributions from factors such as ligand volume, shape and flexibility. To further verify the observed trends here, more complete models for functionalized nanoparticles can be developed and explored at least for the insertion step, similar to previous studies.[15,29,51] Further analysis of the ejection step with more complex models for the nanoparticle and membrane remains computationally challenging and is perhaps best conducted with experimental studies, provided that the relevant ligand distributions can be realized.[64]

4 Conclusions

Most, if not all, design strategies for nanoparticle internalization are based on equilibrium considerations. Biological transport, however, often relies on non-equilibrium processes. In this study, motivated by recent studies of Raines and co-workers on protein delivery based on bioreversible esterification,[47] we use computational models to explore the effectiveness of a similar non-equilibrium transport mechanism for nanoparticles across the lipid membrane.

View Article Online
DOI: 10.1039/D3NR00930K

With coarse-grained models, we demonstrate that the non-equilibrium mechanism can be robust. Moreover, we explore a few basic parameters related to the properties and distributions of surface ligands to identify relevant design rules that govern the efficiency of the transport.

We divide the transport process into insertion and ejection steps, which are studied with different coarse-grained models using free energy and reactive Monte Carlo simulations, respectively. For the non-equilibrium transport to be effective, both steps need to be considered. Our simulations show that the transport efficiency is relatively insensitive to the fraction of reactive surface ligands once a modest threshold is surpassed, while the distribution pattern of different (hydrophilic, reactive and permanent hydrophobic) ligands has a notable impact on both the insertion and ejection steps. For example, random and Janus distributions of hydrophilic and hydrophobic surface ligands, or polar distribution of reactive surface ligands with a hydrophobic equatorial domain are not expected to be effective due to potential difficulties associated with insertion and ejection steps, respectively. On the other hand, it is likely effective to mix hydrophilic and hydrophobic ligands with the former in the polar or equatorial regions, while the reactive ligands being distributed in a Janus-like pattern in the hydrophobic domain. Our study thus highlights the value of rational design of surface functionalization for efficient non-equilibrium transport and provides a set of relevant guidelines. With additional extensions, such as more realistic treatment of the membrane environment, the computational framework established in our work can be used to analyze the non-equilibrium transport of biomolecules and nanomaterials across complex membranes.

Conflict of Interest Statement

There are no conflicts of interest to declare.

View Article Online
DOI: 10.1039/D3NR00930K

Acknowledgement

This material is based upon work supported by the National Science Foundation under Grant No. CHE-2001611, the NSF Center for Sustainable Nanotechnology. The CSN is part of the Centers for Chemical Innovation Program. The authors acknowledge discussions with Prof. Ron Raines, who brought our attention to this interesting research topic. We also thank Prof. M. Lund for providing the Faunus program, which was used for the reactive Monte Carlo sampling, and for interesting discussions. Computational resources from the Extreme Science and Engineering Discovery Environment (XSEDE[65]), which is supported by NSF grant number ACI-1548562, are greatly appreciated; part of the computational work was performed on the Shared Computing Cluster, which is administered by Boston University's Research Computing Services (URL: www.bu.edu/tech/support/research/).

References

(1) Mitchell, M. J.; Billingsley, M. M.; Langer, R. Engineering precision nanoparticles for drug delivery. *Nat. Rev. Drug Discov.* **2021**, *20*, 101–124.

(2) Anselmo, A. C.; Mitragotri, S. Nanoparticles in the clinic: An update. *Bioeng. & Trans. Medi.* **2019**, *4*, e10143.

(3) Murphy, C. J.; Vartanian, A. M.; Geiger, F. M.; Hamers, R. J.; Pedersen, J.; Cui, Q.; Haynes, C. L.; Carlson, E. E.; Hernandez, R.; R. D. Klaper et al. Biological Responses to Engineered Nanomaterials: Needs for the Next Decade. *ACS Central Sci.* **2015**, *1*, 117–123.

(4) Zhang, S.; Gao, H.; Bao, G. Physical principles of nanoparticle cellular endocytosis. *ACS Nano* **2015**, *9*, 8655–8671.

(5) Tang, H.; Ye, H.; Zhang, H.; Zheng, Y. Aggregation of nanoparticles regulated by mechanical properties of nanoparticle–membrane system. *Nanotech.* **2018**, *29*, 405102.

View Article Online
DOI: 10.1039/D3NR00930K

(6) Singhal, A.; Sevink, G. J. A. The role of size and nature in nanoparticle binding to a model lung membrane: an atomistic study. *Nano. Adv.* **2021**, *3*, 6635–6648.

(7) Lunnoo, T.; Assawakhajornsak, J.; Puangmali, T. In Silico Study of Gold Nanoparticle Uptake into a Mammalian Cell: Interplay of Size, Shape, Surface Charge, and Aggregation. *J. Phys. Chem. C* **2019**, *123*, 3801–3810.

(8) Faried, M.; Suga, K.; Okamoto, Y.; Shameli, K.; Miyake, M.; Umakoshi, H. Membrane Surface-Enhanced Raman Spectroscopy for Cholesterol-Modified Lipid Systems: Effect of Gold Nanoparticle Size. *ACS Omega* **2019**, *4*, 13687–13695.

(9) Nowak, M.; Brown, T. D.; Graham, A.; Helgeson, M. E.; Mitragotri, S. Size, shape, and flexibility influence nanoparticle transport across brain endothelium under flow. *Bioeng. & Trans. Medi.* **2020**, *5*, e10153.

(10) Vacha, R.; Martinez-Veracoechea, F. J.; Frenkel, D. Receptor-Mediated Endocytosis of Nanoparticles of Various Shapes. *Nano Lett.* **2011**, *11*, 5391–5395.

(11) Shen, Z.; Ye, H.; Yi, X.; Li, Y. Membrane Wrapping Efficiency of Elastic Nanoparticles during Endocytosis: Size and Shape Matter. *ACS Nano* **2019**, *13*, 215–228.

(12) Carnovale, C.; Bryant, G.; Shukla, R.; Bansal, V. Identifying Trends in Gold Nanoparticle Toxicity and Uptake: Size, Shape, Capping Ligand, and Biological Corona. *ACS Omega* **2019**, *4*, 242–256.

(13) Wang, W.; Gaus, K.; Tilley, R. D.; Gooding, J. J. The impact of nanoparticle shape on cellular internalisation and transport: what do the different analysis methods tell us? *Mater. Horiz.* **2019**, *6*, 1538–1547.

(14) Lee, D. U.; Park, J.-Y.; Kwon, S.; Park, J. Y.; Kim, Y. H.; Khang, D.; Hong, J. H. Apoptotic lysosomal proton sponge effect in tumor tissue by cationic gold nanorods. *Nanoscale* **2019**, *11*, 19980–19993.

View Article Online
DOI: 10.1039/D3NR00930K

(15) R. C. van Lehn; Alexander-Katz, A. Grafting Charged Species to Membrane-Embedded Scaffolds Dramatically Increases the Rate of Bilayer Flipping. *ACS Central Sci.* **2017**, *3*, 186–195.

(16) R. C. van Lehn; Alexander-Katz, A. Membrane-Embedded Nanoparticles Induce Lipid Rearrangements Similar to Those Exhibited by Biological Membrane Proteins. *J. Phys. Chem. B* **2014**, *118*, 12586–12598.

(17) R. C. van Lehn; Ricci, M.; Silva, P. H. J.; Andreozzi, P.; Reguera, J.; Voitchovsky, K.; Stellacci, F.; Alexander-Katz, A. Lipid tail protrusions mediate the insertion of nanoparticles into model cell membranes. *Nat. Commun.* **2013**, *5*, 4482.

(18) R. C. van Lehn; Atukorale, P. U.; Carney, R. P.; Yang, Y.-S.; Stellacci, F.; Irvine, D. J.; Alexander-Katz, A. Effect of Particle Diameter and Surface Composition on the Spontaneous Fusion of Monolayer-Protected Gold Nanoparticles with Lipid Bilayers. *Nano Lett.* **2013**, *13*, 4060–4067.

(19) Zhang, Y. Q.; Dahal, U.; Feng, Z. V.; Rosenzweig, Z.; Cui, Q.; Hamers, R. J. Influence of Hydrophobic Length and Flexibility of Surface Ligands on Phospholipid Membrane Disruption by Cationic Nanoparticles. *Langmuir* **2021**, *37*, 7600–7610.

(20) Zou, D.; Wu, Z.; Yi, X.; Hui, Y.; Yang, G.; Liu, Y.; Wang, T. H.; Brooks, A.; Wang, H.; Liu, X.; Xu, Z. P.; Roberts, M. S.; Gao, H.; Zhao, C. Nanoparticle elasticity regulates the formation of cell membrane-coated nanoparticles and their nano-bio interactions. *Proc. Natl. Acad. Sci. U.S.A.* **2023**, *120*, e2214757120.

(21) Kesner, L. A.; Piskulich, Z. A.; Cui, Q.; Rosenzweig, Z. Untangling the Interactions between Anionic Polystyrene Nanoparticles and Lipid Membranes Using Laurdan Fluorescence Spectroscopy and Molecular Simulations. *J. Am. Chem. Soc.* **2023**, *145*, 7962–7973.

View Article Online
DOI: 10.1039/D3NR00930K

(22) Wang, X.; Li, L.; Song, F. Interplay of Nanoparticle Properties during Endocytosis. *Crystals* **2021**, *11*, 728.

(23) Bahrami, A. H.; Weikl, T. R. Curvature-Mediated Assembly of Janus Nanoparticles on Membrane Vesicles. *Nano Lett.* **2018**, *18*, 1259–1263.

(24) Yan, Z.; Wu, Z.; Li, S.; Zhang, X.; Yi, X.; Yue, T. Curvature-mediated cooperative wrapping of multiple nanoparticles at the same and opposite membrane sides. *Nanoscale* **2019**, *11*, 19751–19762.

(25) Wiemann, J. T.; Shen, Z.; Ye, H.; Li, Y.; Yu, Y. Membrane poration, wrinkling, and compression: deformations of lipid vesicles induced by amphiphilic Janus nanoparticles. *Nanoscale* **2020**, *12*, 20326–20336.

(26) Ding, H.-m.; Tian, W.-d.; Ma, Y.-q. Designing Nanoparticle Translocation through Membranes by Computer Simulations. *ACS Nano* **2012**, *6*, 1230–1238.

(27) Qian, L.; Fu, J.; Yuan, P.; Du, S.; Huang, W.; Li, L.; Yao, S. Q. Intracellular Delivery of Native Proteins Facilitated by Cell-Penetrating Poly(disulfide)s. *Angew. Chem. Int. Ed.* **2018**, *57*, 1532–1536.

(28) Pishkenari, H. N.; Barzegar, M. R.; Taghibakhshi, A. Study and Simulation of Nanoparticle Translocation Through Cell Membrane. *Iran. J. Sci. & Techno, Trans. of Mech. Engr.* **2019**, 1–22.

(29) Chew, A. K.; Pedersen, J. A.; R. C. van Lehn Predicting the Physicochemical Properties and Biological Activities of Monolayer-Protected Gold Nanoparticles Using Simulation-Derived Descriptors. *ACS Nano* **2022**, *16*, 6282–6292.

(30) Bahrami, A. H.; Lipowsky, R.; Weikl, T. R. The role of membrane curvature for the wrapping of nanoparticles. *Soft Matt.* **2016**, *12*, 581–587.

View Article Online
DOI: 10.1039/D3NR00930K

(31) Spangler, E. J.; Upreti, S.; Laradji, M. Partial wrapping and spontaneous endocytosis of spherical nanoparticles by tensionless lipid membranes. *J. Chem. Phys.* **2016**, *144*, 044901.

(32) Agudo-Canalejo, J.; Lipowsky, R. Critical particle sizes for the engulfment of nanoparticles by membranes and vesicles with bilayer asymmetry. *ACS Nano* **2015**, *9*, 3704–3720.

(33) Ambjörnsson, T.; Metzler, R. Chaperone-assisted translocation. *Phys. Biol.* **2004**, *1*, 77.

(34) Suhonen, P. M.; Linna, R. P. Chaperone-assisted translocation of flexible polymers in three dimensions. *Phys. Rev. E* **2016**, *93*, 012406.

(35) Emamyari, S.; Fazli, H. Polymer translocation through a nanopore in the presence of chaperones: A three dimensional MD simulation study. *Comput. Conds. Matt.* **2017**, *13*, 96–103.

(36) Vale, R. D.; Oosawa, F. Protein motors and Maxwell's demons: Does mechanochemical transduction involve a thermal ratchet? *Adv. Biophys.* **1990**, *26*, 97–134.

(37) Luo, K.; Ala-Nissila, T.; Ying, S.-C.; Metzler, R. Driven polymer translocation through nanopores: Slow-vs.-fast dynamics. *EuroPhys. Lett.* **2009**, *88*, 68006.

(38) Kwon, S.; Sung, B. J. Effects of solvent quality and non-equilibrium conformations on polymer translocation. *J. Chem. Phys.* **2018**, *149*, 244907.

(39) Katkar, H. H.; Muthukumar, M. Role of non-equilibrium conformations on driven polymer translocation. *J. Chem. Phys.* **2018**, *148*, 024903.

(40) Sakaue, T. Dynamics of Polymer Translocation: A Short Review with an Introduction of Weakly-Driven Regime. *Polymers* **2016**, *8*, 424.

(41) Lv, J.; Fan, Q.; Wang, H.; Cheng, Y. Polymers for Cytosolic Protein Delivery. *Biomater.* **2019**, *218*, 119358.

View Article Online
DOI: 10.1039/D3NR00930K

(42) de Oliveira, E. C. L.; Santana, K.; Josino, L.; Lima, A. H. L.; Junior, C. S. S. Predicting cell-penetrating peptides using machine learning algorithms and navigating in their chemical space. *Sci. Rep.* **2021**, *11*, 7628.

(43) Kwon, S.; Lee, S.; Cho, H. W.; Kim, J.; Kim, J. S.; Sung, B. J. The breakdown of the local thermal equilibrium approximation for a polymer chain during packaging. *J. Chem. Phys.* **2019**, *150*, 204901.

(44) Fuchs, S. M.; Raines, R. T. Arginine Grafting to Endow Cell Permeability. *ACS Chem. Biol.* **2007**, *2*, 167–170.

(45) Palte, M. J.; Raines, R. T. Interaction of Nucleic Acids with the Glycocalyx. *J. Am. Chem. Soc.* **2012**, *134*, 6218–6223.

(46) Andersen, K. A.; Smith, T. P.; Lomax, J. E.; Raines, R. T. Boronic Acid for the Traceless Delivery of Proteins into Cells. *ACS Chem. Biol.* **2016**, *11*, 319–323.

(47) Mix, K. A.; Lomax, J. E.; Raines, R. T. Cytosolic Delivery of Proteins by Bioreversible Esterification. *J. Am. Chem. Soc.* **2017**, *139*, 14396–14398.

(48) Marrink, S. J.; Monticelli, L.; Melo, M. N.; Alessandri, R.; Tieleman, D. P.; Souza, P. C. T. Two decades of Martini: Better beads, broader scope. *WIREs Comput. Mol. Sci.* **2023**, *13*, e1620.

(49) Johnson, J. K.; Panagiotopoulos, A. Z.; Gubbins, K. E. Reactive canonical Monte Carlo. *Mol. Phys.* **1994**, *81*, 717–733.

(50) Marrink, S. J.; Risselada, H. J.; Yefimov, S.; Tieleman, D. P.; Vries, A. H. d. The MARTINI Force Field: Coarse Grained Model for Biomolecular Simulations. *J. Phys. Chem. B* **2007**, *111*, 7812 – 7824.

(51) Das, M.; Dahal, U.; Mesele, O.; Liang, D. Y.; Cui, Q. Molecular Dynamics Simulation

View Article Online
DOI: 10.1039/D3NR00930K

of Interaction between Functionalized Nanoparticles with Lipid Membranes: Analysis of Coarse-grained Models. *J. Phys. Chem. B* **2019**, *123*, 10547–10561.

(52) Hsu, P.; Bruininks, B. M. H.; Jefferies, D.; Souza, P. C. T. d.; Lee, J.; Patel, D. S.; Marrink, S. J.; Qi, Y.; Khalid, S.; Im, W. CHARMM-GUI Martini Maker for modeling and simulation of complex bacterial membranes with lipopolysaccharides. *J. Comput. Chem.* **2017**, *38*, 2354–2363.

(53) Qi, Y.; Ingolfsson, H. I.; Cheng, X.; Lee, J.; Marrink, S. J.; Im, W. CHARMM-GUI Martini Maker for Coarse-Grained Simulations with the Martini Force Field. *J. Chem. Theory Comput.* **2015**, *11*, 4486–4494.

(54) Jo, S.; Kim, T.; Iyer, V. G.; Im, W. CHARMM-GUI: A web-based graphical user interface for CHARMM. *J. Comput. Chem.* **2008**, *29*, 1859–1865.

(55) Abraham, M. J.; Murtola, T.; Schulz, R.; Páll, S.; Smith, J. C.; Hess, B.; Lindahl, E. GROMACS: High performance molecular simulations through multi-level parallelism from laptops to supercomputers. *SoftwareX* **2015**, *1*, 19–25.

(56) Van Gunsteren, W. F.; Berendsen, H. J. C. A Leap-frog Algorithm for Stochastic Dynamics. *Mol. Simul.* **1988**, *1*, 173–185.

(57) Bussi, G.; Donadio, D.; Parrinello, M. Canonical sampling through velocity rescaling. *J. Chem. Phys.* **2007**, *126*, 014101.

(58) Berendsen, H. J. C.; Postma, J. P. M.; Gunsteren, W. F. v.; DiNola, A.; Haak, J. R. Molecular dynamics with coupling to an external bath. *J. Chem. Phys.* **1984**, *81*, 3684–3690.

(59) Parrinello, M.; Rahman, A. Polymorphic transitions in single crystals: A new molecular dynamics method. *J. Appl. Phys.* **1981**, *52*, 7182–7190.

View Article Online
DOI: 10.1039/D3NR00930K

(60) Kumar, S.; Rosenberg, J. M.; Bouzida, D.; Swendsen, R. H.; Kollman, P. A. Multidimensional free-energy calculations using the weighted histogram analysis method. *J. Comput. Chem.* **1995**, *16*, 1339–1350.

(61) Lund, M.; Trulsson, M.; Persson, B. Faunus: An object oriented framework for molecular simulation. *Source Code for Biology and Medicine* **2008**, *3*, 1–1.

(62) Stenqvist, B.; Thuresson, A.; Kurut, A.; Vácha, R.; Lund, M. Faunus - a flexible framework for Monte Carlo simulation. *Mol. Simul.* **2013**, *39*, 1233–1239.

(63) MacCallum, J. L.; Bennett, W. F. D.; Tieleman, D. P. Distribution of amino acids in a lipid bilayer from computer simulations. *Biophys. J.* **2008**, *94*, 3393–3404.

(64) Pengo, P.; Sologan, M.; Pasquato, L.; Guida, F.; Pacor, S.; Tossi, A.; Stellacci, F.; Marson, D.; Boccardo, S.; Pricl, S.; Posocco, P. Gold nanoparticles with patterned surface monolayers for nanomedicine: current perspectives. *Eur. Biophys. J. Biophys. Lett.* **2017**, *46*, 749–771.

(65) Towns, J.; Cockerill, T.; Dahan, M.; Foster, I.; Gaither, K.; Grimshaw, A.; Hazelwood, V.; Lathrop, S.; Lifka, D.; Peterson, G. D.; Roskies, R.; Scott, J. R.; Wilkins-Diehr, N. XSEDE: Accelerating Scientific Discovery. *Comput Sci. & Engn.* **2014**, *16*, 62–74.